Paek, Min; Kim, Kyung-Ho; Lindberg, Daniel; Pak, Jong-Jin

Formation of nitride and oxide inclusions in liquid Fe-Cr-Ti-Al alloys

Published in:
Steel Research International

DOI:
10.1002/srin.202000508

Published: 26/11/2020

Document Version
Peer-reviewed accepted author manuscript, also known as Final accepted manuscript or Post-print

Please cite the original version:
Paek, M., Kim, K.-H., Lindberg, D., & Pak, J.-J. (2020). Formation of nitride and oxide inclusions in liquid Fe-Cr-Ti-Al alloys. *Steel Research International*, Article 2000508. https://doi.org/10.1002/srin.202000508

Formation of Nitride and Oxide Inclusions in Liquid Fe-Cr-Ti-Al Alloys

Min-Kyu Paek,[a*] Kyung-Ho Kim,[b] Daniel Lindberg,[a] and Jong-Jin Pak[c]

[a] Department of Chemical and Metallurgical Engineering, Aalto University, Espoo, 02150, Finland

[b] Melting Department, Hitachi Metals, Ltd., Yasugi, 692-8601, Japan

[c] Department of Materials Science and Chemical Engineering, Hanyang University, ERICA, Ansan, 15588, Korea

*Corresponding author: min.paek@aalto.fi

Abstract:

Thermodynamics of nitride and oxide inclusion formations in liquid Fe-Cr alloys containing Ti and Al was studied to provide accurate information for the refining process of ferritic stainless steel. The compatible set of the interaction parameters for the multicomponent Fe-Cr-Ti-Al-N-O system was tabulated based on Wagner's formalism. The selected parameters were valid to reproduce the thermodynamic behavior of N and O in both Fe-Cr-Ti-Al-N and Fe-Cr-Ti-Al-O systems. The verification experiments of the N solubilities and nitride solubility products in Fe-Cr-Ti-N, Fe-Cr-Al-N, and Fe-Cr-Ti-Al-N melts were in good agreement with the present calculations over the wide range of melt composition and temperature. The various types of Ti nitride inclusions were observed in Fe-Cr-Ti-Al-N melt during cooling. The inclusion evolution experiment was also carried out to confirm the morphology and composition change of oxide inclusions by the Al-Ti complex deoxidation in liquid Fe-Cr alloy. The relation between the melt composition and the stability of oxide inclusion was thermodynamically described by constructing of the equilibrium predominance diagram in the Fe-Cr-Ti-Al-O system.

Keywords: ferritic stainless steel, nitride, oxide, Wagner's formalism, interaction parameter

1. Introduction

Low carbon and nitrogen ferritic stainless steels provide good corrosion resistance, high formability, and weldability.[1,2] In the absence of solid-state phase transformation, the achievement of grain refinement has been crucial for the fabrication of high-quality components using such fully ferritic steels by arc welding. The addition of Ti is known to help the transition from columnar to equiaxed cast structure by forming fine secondary inclusions such as TiN, TiC, and TiO_x aiding heterogeneous nucleation.[3-5] Al is also added after the decarburization process as a typical deoxidant as well as a reductant for the formed Cr_2O_3 layer.[6] Since Ti and Al have a significantly strong affinity with both N and O in the stainless steel melts, various types of nitrides (TiN and AlN) and oxide inclusions (Ti_3O_5, Ti_2O_3, Al_2O_3, $MgAl_2O_4$, *etc.*) can be formed. However, an excessive formation of such inclusions can lower the productivity by clogging the submerged entry nozzle during the continuous casting process and ridging problem during cold-press forming.[7] Therefore, accurate thermodynamic information of liquid Fe-Cr-Ti-Al alloy has to be secured to precisely control the inclusion formation during the refining process and the solidification structure of the final product of ferritic stainless steels.

To understand the formation of nitride and oxide inclusions in the core system of ferritic stainless steelmaking, the consistent set of N and O parameters in the Fe-Cr-Ti-Al-N-O and its sub-systems has been determined for the last decade by the authors' recent studies. Wagner's formalism[8] has been adopted to provide high accessibility using the simple equations of interaction parameters not only for academia but also for the steel industry. In the systems containing N, the N solubility and solubility product of TiN and AlN have been measured in Fe-Cr-Ti-Al-N melt over a wide range of melt composition and temperature.[9-11] The simultaneous effects of two different alloying elements on the N solubility were determined from the experimental results, and the reproducibility of the N content was improved in the multicomponent system by considering the cross-product effect.[9] Meanwhile, for the O containing systems, the deoxidation equilibria in Fe-Cr-Ti-Al-O melt have been measured to determine the thermodynamic relation between alloying elements and O in liquid iron.[12] However, it was thermodynamically analyzed only recently due to the complexity of the O behavior in liquid iron alloys.

Figure 1 compares the equilibrium Ti-N reaction with Ti-O relation in liquid iron at 1600 °C. In the Fe-Ti-N system, the effect of Ti on N in liquid iron can be directly determined by the N_2

gas/liquid metal equilibrium reaction. There is a measurable region of the N solubility data with the Ti addition (dotted line) before the formation of TiN (solid line), as shown in Figure 1a. The increasing tendency of the N solubility with the Ti content can be described by the negative interaction parameter of Ti on N in liquid iron, $e_{\mathrm{N}}^{\mathrm{Ti}}$ = -0.21.[13] On the other hand, in the Fe-Ti-O system, Ti oxide is formed over the entire Ti concentration range even from a single ppm, as can be seen in Figure 1b. It is impossible to purely measure the interaction between Ti and O in liquid iron by the O_2 gas/liquid metal equilibration without the formation of Ti oxide, and hence the interaction parameter of Ti on O in liquid iron, $e_{\mathrm{O}}^{\mathrm{Ti}}$ = -0.63[14] was determined by measuring the solubility product of Ti and O under the Ti_3O_5 or Ti_2O_3 saturated condition. In both systems, the same interaction parameter, such as the specific effect of Cr on Ti, $e_{\mathrm{Ti}}^{\mathrm{Cr}}$ can be determined by measuring the change of Ti activity with the addition of Cr under the saturation conditions of Ti nitride and oxide, respectively. However, the Ti deoxidation experiments (Figure 1b)[14-20] are significantly scattered compared to the data measured under the TiN saturated condition (Figure 1a).[13,21-23] Therefore, in the authors' recent study,[9] the interactions between alloying elements such as Cr-Ti, Cr-Al, and Al-Ti have been determined by the relatively stable metal/nitride/gas equilibrium results. These specific parameters should be compatible with the same base alloy system regardless of the impurities, so they were applied to describe both nitride and oxide formation in Fe-Cr-Ti-Al alloy melts.

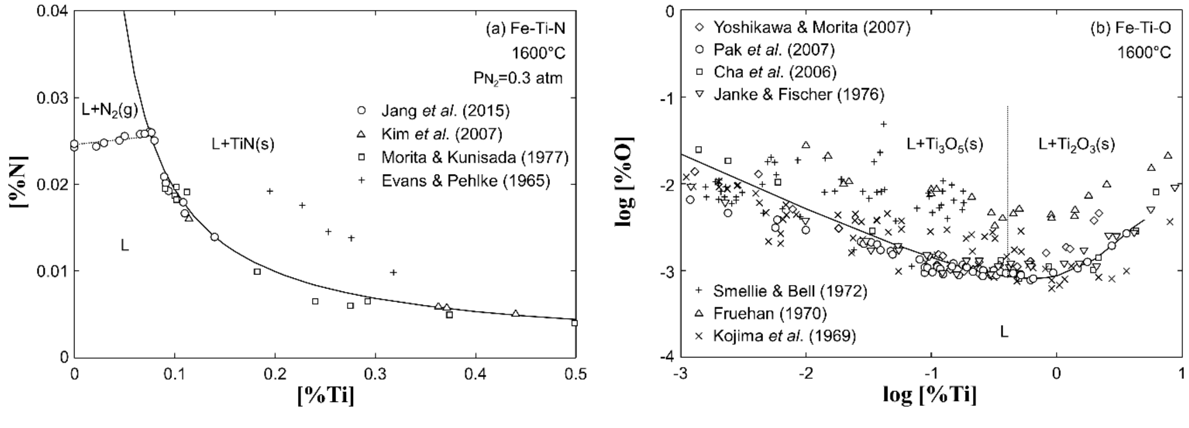

Figure 1. Calculated a) Ti-N and b) Ti-O relation at 1600 °C in liquid iron along with the experimental results.[13-23]

Thermodynamic parameters selected from the authors' recent studies[9-14,24,25] and previous reports[26-30] are listed in **Table 1** for the multicomponent Fe-Cr-Ti-Al-N-O system. The present study carried out the verification experiments in the Fe-Cr-Ti-Al-N and Fe-Cr-Ti-Al-O systems, respectively, for checking the validity and compatibility of the parameters. In the N containing systems, the N solubility and the solubility product of TiN and AlN were measured with changing the composition or temperature. The extracted nitride inclusions in Fe-18 wt%Cr-0.28 wt%Al-Ti-N melt during cooling were characterized. Also, the inclusion evolution experiment was carried out by adding the deoxidants of Al and Ti in sequence at 1600 °C in Fe-18 wt%Cr-Ti-Al-O melt. The chemistry of the formed inclusions was characterized and compared with the equilibrium predominance diagram constructed in the Fe-Cr-Ti-Al-O system.

Table 1. The first- and second-order interaction parameters in Fe-Cr-Ti-Al-N-O system.

e_i^j	Al	Cr	N	O	Ti
Al	0.043 [24]	0.017 [9]	0.033 [24]	-1.98 [27]	-0.011 [9]
Cr	-	0 [29]	-	-	-
N	0.017 [24]	-0.06 [25] (-147.8/T+0.019)	0 [30]	-	-0.21 [13]
O	-1.17 [27]	-0.032 [29] (-123/T+0.034)	-	-0.17 [28] (-1750/T+0.76)	-0.54 [14] (-1642/T+0.3358)
Ti	-0.024 [9]	0.024 [11] (406.7/T-0.1933)	-0.72 [13]	-1.62 [14] (-4915/T+1.005)	0.048 [13]
r_i^j	Al	Cr	N	O	Ti
Al	0 [24]	0 [9]	0 [24]	0 [27]	0 [9]
Cr	-	0 [29]	-	-	-
N	0 [24]	0.0007 [25] (-2.58/T+0.0021)	0 [30]	-	0 [13]
O	0 [27]	0 [29]	-	0 [29]	0.0385 [14]
Ti	0 [9]	0 [11] (-20.6/T-0.011)	0 [13]	-0.355 [14]	0 [13]
$r_i^{j,k}$	Al,Cr	Al,Ti	Cr,Ti		
N	-0.003 [9]	0 [9]	0 [9]		

2. Experimental Procedures

2.1. Gas-Liquid Metal-Nitride Equilibration

The N solubility and nitride solubility product in Fe-Cr-Ti-N, Fe-Cr-Al-N, and Fe-Cr-Ti-Al-N melts were measured by using the gas-liquid metal and gas-liquid metal-nitride equilibration techniques, respectively. Five hundred grams of electrolytic iron (99.99 %purity) charged in a fused alumina crucible (outer diameter (OD): 56 mm, inner diameter (ID): 50 mm, and height (H): 96 mm) were melted using a 15 kW/30 kHz high-frequency induction furnace. The melt temperature was measured by immersing Pt/Pt-13 wt%Rh thermocouple sheathed with the closed one end alumina tube (OD: 6 mm). Since O retards the N dissolution rate as a surface-active element of liquid iron, the initial O content was forcibly controlled below 20 ppm in liquid iron by blowing the Ar-10 %H_2 gas mixture for 4 hours. Then, the gas flow rate of N_2 and Ar-10 %H_2 gases was adjusted to keep the reduced N_2 partial pressure. After checking the N solubility, high purity alloys such as Cr (99.95 %purity), Ti (99.995 %purity), or Al (99.99 %purity) shots were added. A new equilibrium N content was attained within 1 hour, which was confirmed by the sampling using a 4 mm ID quartz tube connected to a syringe (10 mL) and *in-situ* analysis using the N/O analyzer. The alloys were continuously added to reach the desired composition. The effects of composition and temperature on the solubility product of the nitride formation were determined by adding alloys or changing temperatures.

2.2. Al-Ti Complex Deoxidation

The evolution of inclusion during the Al-Ti complex deoxidation in Fe-Cr-Ti-Al-O melt was measured by checking the morphology and chemistry changes with time. Five hundred grams of Fe-18 wt%Cr alloy were melted in a MgO crucible at 1600 °C. After melting, the initial O content in the alloy was controlled to have the target value of 300 ppm by the addition of Fe_2O_3 powder (99.99 %purity) and blowing the Ar-10 %H_2 gas mixture. Then, the gas was switched to the purified Ar gas which was dehydrated and deoxidized by passing through phosphorus pentoxide cylinder and pre-heated furnace charged with sponge Ti (99.9 %purity), respectively. As the first deoxidant, the Al shot was added under the purified Ar atmosphere. After 8 min, the sample was extracted by the quartz tube and rapidly quenched in ice water. The Ti addition was followed immediately, and then the sampling was also performed at 30 sec, 1 min, 3 min, 5 min, 10 min, and 20 min after the Ti addition.

2.3. Analyses

The quenched samples were sectioned and polished for the chemical analyses. The N and O contents of the metal samples were measured by the inert gas fusion – infrared absorptiometry technique using the N/O analyzer (LECO TC–600). The concentration of metallic elements such as Cr, Ti, and Al was analyzed by the Inductively Coupled Plasma – Atomic Emission Spectroscopy (ICP–AES, SPECTRO ARCOS). The nitride inclusions precipitated in the melts were extracted from the metal samples by the potentiostatic technique using the Pt electrode in the 10 pct acetyl-acetone solution (AA). After completing the dissolution of a metal sample (~0.5 g), the suspended inclusions in the AA solution were collected by the filtration using a fine membrane filter with 0.1 μm open pores. The filter was then dried in a vacuum desiccator and coated by the Pt plasma beam whole with the sample holder to avoid any dust or particles gathered on it. For the observation of oxide inclusions, the metal samples were cross-sectioned and polished using the water-free alcohol and diamond suspension. The morphology and composition of inclusions were analyzed by the Scanning Electron Microscopy – Energy Dispersive X-ray Sectroscopy (SEM–EDS, Hitachi S4800).

3. Results and Discussion

3.1. N Solubility and Nitride Formation in Fe-Cr-Ti-Al-N Melt

Ti and Al are strong nitride formers. As shown in Figure 1a, the N solubility linearly increases with the Ti addition under a given N_2 partial pressure before the formation of TiN. When the melt is saturated with TiN, the equilibrium N content deceases with Ti addition according to the equilibrium solubility product of TiN by Equations (3) and (4). In the TiN saturated condition, the N content can be controlled by the adjusted N_2 partial pressure between the TiN layer and liquid metal. The addition of a third alloying element, such as Cr, will simultaneously change the activities of Ti and N under the TiN saturation. Thus, from the change of the TiN solubility product, the specific effect of Cr on Ti in liquid iron can be determined. In the authors' recent study,[9] the specific effect of Cr on Al in liquid iron was also determined by measuring the AlN solubility product with the addition of Cr. The accuracy of these thermodynamic relations between the alloying elements (*e.g.*, Cr-Ti and Cr-Al) is very important because they can also be used to describe the effect of Cr on the deoxidation equilibria in liquid iron alloys. Therefore, the validity of the parameters was checked by measuring the solubility product of TiN and AlN in Fe-Cr-Ti-N and Fe-Cr-Al-N melts, respectively.

The thermodynamic behavior of N can be expressed by the following equilibrium reactions for the dissolution of N_2 gas, pure solid TiN, and AlN in liquid iron:

$$\frac{1}{2}\mathrm{N_2(g)} = \underline{\mathrm{N}} \tag{1}$$

$$K_{\mathrm{N}} = \frac{f_{\mathrm{N}}[\%\mathrm{N}]}{P_{\mathrm{N_2}}^{1/2}} \tag{2}$$

$$\mathrm{TiN(s)} = \underline{\mathrm{Ti}} + \underline{\mathrm{N}} \tag{3}$$

$$K_{\mathrm{TiN}} = \frac{h_{\mathrm{Ti}} h_{\mathrm{N}}}{a_{\mathrm{TiN}}} = \frac{f_{\mathrm{Ti}} f_{\mathrm{N}}[\%\mathrm{Ti}][\%\mathrm{N}]}{a_{\mathrm{TiN}}} \tag{4}$$

$$\mathrm{AlN(s)} = \underline{\mathrm{Al}} + \underline{\mathrm{N}} \tag{5}$$

$$K_{\mathrm{AlN}} = \frac{h_{\mathrm{Al}} h_{\mathrm{N}}}{a_{\mathrm{AlN}}} = \frac{f_{\mathrm{Al}} f_{\mathrm{N}}[\%\mathrm{Al}][\%\mathrm{N}]}{a_{\mathrm{AlN}}} \tag{6}$$

where K is the equilibrium constant of the reactions. $P_{\mathrm{N_2}}$ is the controlled N_2 partial pressure, and a_i is the activity of nitride phases. h_i, f_i, and $[\%i]$ are the Henrian activity, Henrian activity coefficient, and the equilibrium concentration of i in wt%, respectively. The values of $\log K_{\mathrm{N}}$ ($= -188/T - 1.25$) by Pehlke and Elliott[26] and $\log K_{\mathrm{TiN}}$ ($= -12{,}740/T + 4.06$)[13] and $\log K_{\mathrm{AlN}}$ ($= -15{,}850/T + 7.03$)[24] by the authors' recent studies were adopted in this study. a_{TiN} and a_{AlN} were set to unity.

In a Fe-Cr-Ti-Al-N multicomponent melt, the f_{Ti}, f_{Al}, and f_{N} can be expressed as the following relations using Wagner's formalism:[8]

$$\log f_{\mathrm{Ti}} = e_{\mathrm{Ti}}^{\mathrm{Ti}}[\%\mathrm{Ti}] + e_{\mathrm{Ti}}^{\mathrm{N}}[\%\mathrm{N}] + e_{\mathrm{Ti}}^{\mathrm{Al}}[\%\mathrm{Al}] + e_{\mathrm{Ti}}^{\mathrm{Cr}}[\%\mathrm{Cr}] + r_{\mathrm{Ti}}^{\mathrm{Cr}}[\%\mathrm{Cr}]^2 \tag{7}$$

$$\log f_{\mathrm{Al}} = e_{\mathrm{Al}}^{\mathrm{Al}}[\%\mathrm{Al}] + e_{\mathrm{Al}}^{\mathrm{N}}[\%\mathrm{N}] + e_{\mathrm{Al}}^{\mathrm{Ti}}[\%\mathrm{Ti}] + e_{\mathrm{Al}}^{\mathrm{Cr}}[\%\mathrm{Cr}] \tag{8}$$

$$\log f_{\mathrm{N}} = e_{\mathrm{N}}^{\mathrm{Ti}}[\%\mathrm{Ti}] + e_{\mathrm{N}}^{\mathrm{Al}}[\%\mathrm{Al}] + e_{\mathrm{N}}^{\mathrm{Cr}}[\%\mathrm{Cr}] + r_{\mathrm{N}}^{\mathrm{Cr}}[\%\mathrm{Cr}]^2 + r_{\mathrm{N}}^{\mathrm{Cr,Al}}[\%\mathrm{Cr}][\%\mathrm{Al}] \quad (9)$$

where e_i^i is the self-interaction parameter of *i*, and e_i^j and r_i^j are the first- and second-order interaction parameters of *j* on *i* in liquid iron in wt%. The self-interaction parameter of N in liquid iron, $e_{\mathrm{N}}^{\mathrm{N}}$ can be negligible because the N dissolution reaction in liquid iron obeys the Sieverts' law.[30,31] The interaction parameters of N such as e_{N}^{i} and r_{N}^{i} have been determined by the variation of N solubility with the addition of alloying elements, *i* (*i* = Ti, Al, and Cr) in liquid iron.[9,13,24,25] $r_{\mathrm{N}}^{i,j}$ is the second-order interaction parameter of the cross-product on N in liquid iron. Only $r_{\mathrm{N}}^{\mathrm{Cr,Al}}$ indicating the simultaneous effect of Cr and Al on N in liquid iron was considerably big value,[9] which can no longer be ignored in the multicomponent system. The specific effects among the alloying elements, e_{Ti}^{i}, r_{Ti}^{i}, and e_{Al}^{i} have been determined from the change of solubility product by the addition of alloying elements, *i* (*i* = Ti, Al, and Cr) under the TiN or AlN saturated condition, respectively.[9,11,13,24] All the parameters mentioned above have been determined based on the Gibbs free energy of the N dissolution reaction proposed by Pehlke and Elliott.[26] Table 1 summarizes the interaction parameters adopted in the present study.

Using the interaction parameters listed in Table 1, the contour lines of solubility product in Fe-Cr-Ti-N and Fe-Cr-Al-N melts were calculated as shown in **Figures 2**a and b, respectively. In the Fe-Cr-Ti-N system, the solubility product of Ti and N for the formation of TiN was verified over the wide temperature range from 1650 to 1520 °C during cooling. After the equilibrium N solubility of 0.0348 wt% was attained in Fe-20 wt%Cr-0.15 wt%Ti melt under P_{N_2} = 0.01 atm at 1650 °C, the melt temperature was gradually lowered to 1600, 1550, and 1520 °C. TiN was not formed in 1650 and 1600 °C because the melt composition was located below the TiN saturation curves (dashed lines), while the TiN layer covered the melt at lower temperatures. At 1550 and 1520 °C, the melt was equilibrated for 1 hour at each temperature. The solubility product of Ti and N corresponded very well with the calculated TiN contour line as shown in Figure 2a. In the Fe-Cr-Al-N system, the solubility product of Al and N for the AlN formation was confirmed at 1600 °C with increasing Cr content in the melt. As shown in Figure 2b, the present results agreed well with the calculated AlN contour lines in Fe-Cr-Al-N melt containing 13, 15.5, and 18 wt%Cr. It should be noted that disregard of the cross-product effect of Cr and Al on N, $r_{\mathrm{N}}^{\mathrm{Cr,Al}}$ would lead the over- or under-estimation of the $e_{\mathrm{Al}}^{\mathrm{Cr}}$ value to fit the experimental results. Therefore, it is very important to confirm the existence of the cross-product effect on N in all sub-systems.

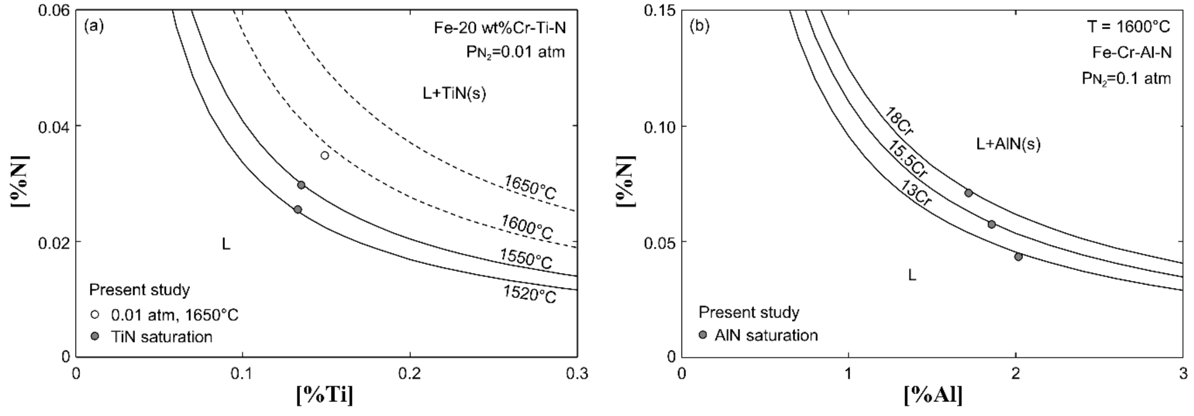

Figure 2. Calculated a) TiN and b) AlN solubility product in liquid Fe-Cr alloys along with the present experimental results.

The change of morphology and chemistry of the nitride inclusions in Fe-Cr-Ti-Al-N melt was also checked during cooling. In order to attain the high equilibrium Ti concentration without forming TiN, the melt was equilibrated at a high temperature of 1700 °C under the reduced N_2 partial pressure of 0.01 atm. The N solubility in Fe-18 wt%Cr-0.28 wt%Al-Ti-N melt increased with the addition of Ti along the predicted N solubility (dotted line) as shown in **Figure 3**. Since the final composition was below the contour line of the TiN solubility product at 1700 °C, no TiN formation was observed after finishing the Ti addition. When the melt temperature was lowered, the thin TiN layer immediately covered the top surface of the melt by reaching the TiN saturated condition. The melt was sampled at 1650 and 1550 °C to check the precipitation of the secondary TiN inclusions during cooling. The inclusions were extracted by the potentiostatic electrolytic method and analyzed by the SEM-EDS analysis. The quantitative data of inclusion composition by EDS were listed in **Table 2**. As shown in **Figures 4**a and b, the samples taken at 1650 °C were identified as the TiN inclusions (~ 2 μm). However, all extracted TiN phases had the Cr solubility in the range from 4.2 to 8.2 wt%. Both TiN and CrN phases are known as the NaCl rock-salt structure Face-Centered Cubic (FCC). Hence Cr can be dissolved by replacing Ti in the substitutional site of (Ti,Cr)(N) solid solution based on the two-sublattice model.[32] In addition, the detected O and C solubility (Figure 4b) can be described by the occupied O and C in the interstitial site of (Ti,Cr)(N,O,C) solid solution because TiO and TiC phases have the same structure with TiN. This observation also implies that the morphology of Ti inclusion would be significantly affected even by a minimal amount of C existed in the high purity raw materials. At 1550 °C, the smaller size (~1 μm) of the cuboid nitride cluster was detected as shown in Figure 4c. Compared to the high-temperature data at 1650 °C, the Cr solubility slightly decreased in the extracted TiN inclusions at 1550 °C, while 2-3 wt% of Al dissolution was observed in some inclusions. The plate shape of inclusion was observed and identified as TiO-rich inclusion with the small solubility of Cr and N. As shown in Figure 4d, the TiC-rich inclusion was also found, which grew to the frame-like structure with a specific crystal direction.

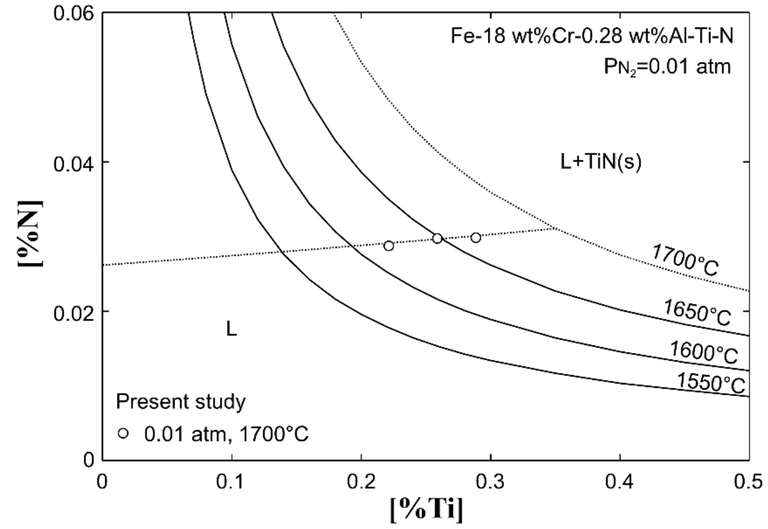

Figure 3. Calculated N solubility and TiN solubility product in Fe-18 wt%Cr-0.28 wt%Al-Ti-N melt at 1550-1700 °C along with the present experimental result at 1700 °C under 0.01 atm.

Table 2. EDS analysis of extracted nitride inclusions from Fe-18 wt%Cr-Ti-Al-N melt.

Extracted temp. (°C)	SEM image	Shape	Chemical formula	Composition (mole fraction)					
				Ti	Cr	Al	N	O	C
1650	Fig. 4a	Hexahedron	(Ti,Cr)N	0.5169	0.0532	-	0.4299	-	-
	Fig. 4b	Hexahedron	(Ti,Cr)(N,C,O)	0.2910	0.0256	-	0.3602	0.1569	0.1663
1550	Fig. 4c	Hexahedron	(Ti,Cr,Al)(N,O)	0.3930	0.0193	0.0371	0.4017	0.1489	-
		Plate	(Ti,Cr)(O,N)	0.2449	0.0135	-	0.1429	0.3999	-
	Fig. 4d	Frame-like	(Ti,Cr)(C,N,O)	0.0944	0.0072	-	0.1887	0.0731	0.6366

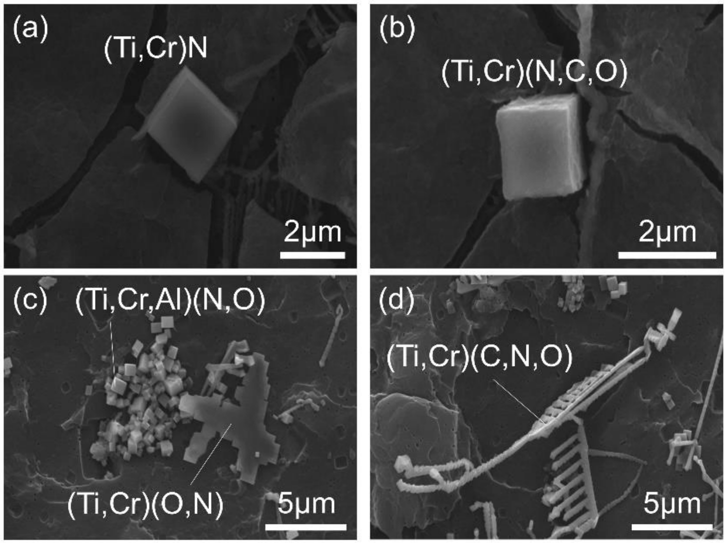

Figure 4. SEM images of extracted nitride inclusions from Fe-18 wt%Cr-0.28 wt%Al-Ti-N melt a & b) at 1650 and c & d) 1550 °C during cooling.

In the present study, the solubility product of Ti and N for the formation of TiN in Fe-Cr-Ti-Al-N melt was calculated under the unit activity of TiN on the assumption that the formed TiN inclusions are all stoichiometric compounds. It was believed that big difference was not anticipated in that regards for the reproducibility of TiN solubility product because the melt was mainly covered with TiN top layer during the entire experiments. Further research is needed on the formation of various types of secondary inclusions suspended in Fe-Cr-Ti-Al-N melts such as Ti nitride, oxy-nitride, and oxy-carbo-nitride with Cr and Al solubilities and vacancy distribution.

3.2. Al-Ti Complex Deoxidation Equilibria in Fe-Cr-Ti-Al-O melt

The formation of oxide inclusions by the addition of Ti or Al cannot be completely avoided due to the significantly strong attraction force between the alloying elements and O in liquid iron as well as the high stability of the oxide phases with very negative Gibbs energy of formation. As shown in Figure 1b, the deoxidation data can be scattered by the existing oxide inclusions in the solidified samples. Since the reproducibility of O analysis strongly depends on the cleanliness of the initial melts, in the authors' recent study,[12] the initial O content in Fe-Cr melt was strictly controlled below 40 ppm to minimize the excessive formation of oxide inclusions. Nevertheless, there were many limitations to determine the proper interaction parameters in the multicomponent system using only deoxidation data. As mentioned earlier, it was required to use the specific parameters of Cr on Ti and Al determined under the stable nitride saturation condition.

The Ti and Al deoxidation equilibria in liquid iron can be expressed, respectively, by the following equilibrium reactions for the dissolution of pure solid Ti_3O_5, Ti_2O_3, and Al_2O_3 in liquid iron:

$$\mathrm{Ti_3O_5(s)} = 3\underline{\mathrm{Ti}} + 5\underline{\mathrm{O}} \tag{10}$$

$$K_{\mathrm{Ti_3O_5}} = \frac{h_{\mathrm{Ti}}^3 h_{\mathrm{O}}^5}{a_{\mathrm{Ti_3O_5}}} = \frac{f_{\mathrm{Ti}}^3 f_{\mathrm{O}}^5 [\%\mathrm{Ti}]^3 [\%\mathrm{O}]^5}{a_{\mathrm{Ti_3O_5}}} \tag{11}$$

$$\mathrm{Ti_2O_3(s)} = 2\underline{\mathrm{Ti}} + 3\underline{\mathrm{O}} \tag{12}$$

$$K_{\mathrm{Ti_2O_3}} = \frac{h_{\mathrm{Ti}}^2 h_{\mathrm{O}}^3}{a_{\mathrm{Ti_2O_3}}} = \frac{f_{\mathrm{Ti}}^2 f_{\mathrm{O}}^3 [\%\mathrm{Ti}]^2 [\%\mathrm{O}]^3}{a_{\mathrm{Ti_2O_3}}} \tag{13}$$

$$\mathrm{Al_2O_3(s)} = 2\underline{\mathrm{Al}} + 3\underline{\mathrm{O}} \tag{14}$$

$$K_{\mathrm{Al_2O_3}} = \frac{h_{\mathrm{Al}}^2 h_{\mathrm{O}}^3}{a_{\mathrm{Al_2O_3}}} = \frac{f_{\mathrm{Al}}^2 f_{\mathrm{O}}^3 [\%\mathrm{Al}]^2 [\%\mathrm{O}]^3}{a_{\mathrm{Al_2O_3}}} \tag{15}$$

where the values of log $K_{\mathrm{Ti_3O_5}}$ (= –72,813/*T* + 21.32) and log $K_{\mathrm{Ti_2O_3}}$ (= –44,238/*T* + 13.0) determined in the authors′ recent study[14] and log $K_{\mathrm{Al_2O_3}}$ (= –64,000/*T* + 20.57) by Rohde *et al.*[27] were adopted in this study. $a_{\mathrm{Ti_3O_5}}$, $a_{\mathrm{Ti_2O_3}}$, and $a_{\mathrm{Al_2O_3}}$ were set to unity.

In a Fe-Cr-Ti-Al-O multicomponent melt, f_{Ti}, f_{Al}, and f_{O} can be expressed as the following relations using Wagner′s formalism:[8]

$$\log f_{\mathrm{Ti}} = e_{\mathrm{Ti}}^{\mathrm{Ti}}[\%\mathrm{Ti}] + e_{\mathrm{Ti}}^{\mathrm{O}}[\%\mathrm{O}] + r_{\mathrm{Ti}}^{\mathrm{O}}[\%\mathrm{O}]^2 + e_{\mathrm{Ti}}^{\mathrm{Al}}[\%\mathrm{Al}] + e_{\mathrm{Ti}}^{\mathrm{Cr}}[\%\mathrm{Cr}] + r_{\mathrm{Ti}}^{\mathrm{Cr}}[\%\mathrm{Cr}]^2 \tag{16}$$

$$\log f_{\mathrm{Al}} = e_{\mathrm{Al}}^{\mathrm{Al}}[\%\mathrm{Al}] + e_{\mathrm{Al}}^{\mathrm{O}}[\%\mathrm{O}] + e_{\mathrm{Al}}^{\mathrm{Ti}}[\%\mathrm{Ti}] + e_{\mathrm{Al}}^{\mathrm{Cr}}[\%\mathrm{Cr}] \tag{17}$$

$$\log f_{\mathrm{O}} = e_{\mathrm{O}}^{\mathrm{O}}[\%\mathrm{O}] + e_{\mathrm{O}}^{\mathrm{Ti}}[\%\mathrm{Ti}] + r_{\mathrm{O}}^{\mathrm{Ti}}[\%\mathrm{Ti}]^2 + e_{\mathrm{O}}^{\mathrm{Al}}[\%\mathrm{Al}] + e_{\mathrm{O}}^{\mathrm{Cr}}[\%\mathrm{Cr}] \tag{18}$$

where the interaction parameters of O ($e_{\mathrm{O}}^{\mathrm{O}}$, $e_{\mathrm{O}}^{\mathrm{Ti}}$, $r_{\mathrm{O}}^{\mathrm{Ti}}$, $e_{\mathrm{O}}^{\mathrm{Al}}$, and $e_{\mathrm{O}}^{\mathrm{Cr}}$) determined by the deoxidation experiments[14,27-29] were adopted, while the self-interaction parameters and specific effects among the alloying elements ($e_{\mathrm{Ti}}^{\mathrm{Ti}}$, $e_{\mathrm{Ti}}^{\mathrm{Cr}}$, $r_{\mathrm{Ti}}^{\mathrm{Cr}}$, $e_{\mathrm{Al}}^{\mathrm{Al}}$, $e_{\mathrm{Al}}^{\mathrm{Ti}}$, and $e_{\mathrm{Al}}^{\mathrm{Cr}}$) determined by the metal/nitride/gas equilibration technique[11-13,24] were applied to describe the deoxidation equilibria in the multicomponent system containing Cr, Ti, and Al.

Using the parameters in Table 1, the Ti-O and Al-O relations in Fe-Cr melt were calculated at 1600 °C as shown in **Figures 5**a and b, respectively. The peaks on the deoxidation curves (dotted lines) represent the transition of the stable oxide phase from Ti_3O_5 to Ti_2O_3 in Fe-Cr-Ti-O melt. The Ti-O and Al-O relations in Fe-Cr melt were compared with the deoxidation curves in liquid iron without Cr (dashed lines). The calculated equilibrium O content increased with increasing Cr content due to the negative interaction between Cr and O in both liquid Fe-Ti and Fe-Al alloys. By adopting the interaction parameters among the alloying elements by the nitride experiments, the Ti deoxidation data in Fe-Cr-Ti-O melt[12,15,33] were in good agreement with the calculated deoxidation curve for Fe-20 wt%Cr alloy as shown in Figure 5a. In the Fe-Cr-Al-O system, most of the Al deoxidation data have been measured using the practical ferritic stainless steels containing Mn, Si, and C. On the other hand, in the authors' recent study,[12] the Al deoxidation equilibria in Fe-16 wt%Cr melt were only measured without any other alloying or contamination. The experimental results over the wide Al concentration range up to 0.81 wt% agreed well with the calculated deoxidation curve in Fe-Cr-Al-O melt at the typical steelmaking temperature of 1600 °C as shown in Figure 5b.

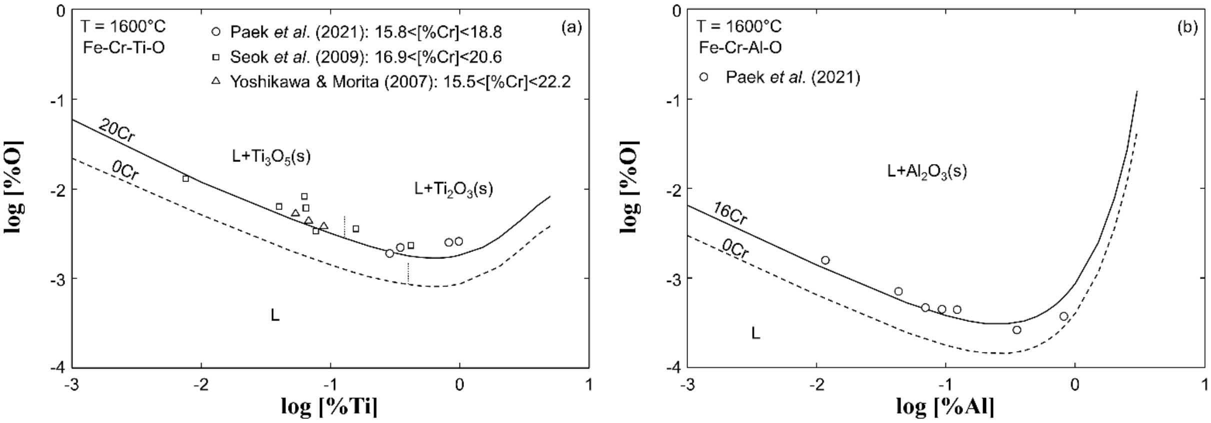

Figure 5. Calculated a) Ti-O and b) Al-O relation in liquid Fe-Cr alloys at 1600 °C along with the experimental results.[12,15,33]

Figure 6 shows the calculated equilibrium predominance diagram for the oxide inclusions in Fe-Cr-Ti-Al-O melt at 1600 °C using the interaction parameters listed in Table 1. To verify the accuracy of the diagram, in the authors' recent study,[12] the Al-Ti complex deoxidation experiments were carried out under the coexisting condition of Al_2O_3 and Ti_3O_5. The measured equilibrium contents of Ti, Al, and O in Fe-18 wt%Cr melt were in good agreement with the calculated phase boundary between Al_2O_3 and Ti_3O_5 as well as the iso-oxygen content lines. In the present study, the inclusion evolution experiment was carried out to check the change of melt composition and inclusion morphology with time for a higher Ti concentration region of Ti_2O_3 saturated condition. **Table 3** summarizes the change of melt composition by adding the deoxidants of Al and Ti in Fe-18 wt%Cr melt with time. Even though the initial O content was 277 ppm O, the total O content was steadily approached to the equilibrium value from 57 to 29 ppm O in 10 min. The Al and Ti contents were quite closely converged with the calculated phase boundary after 20 min as shown in the figure. After the addition of Ti following Al deoxidation, the Al content increased from 70 to 140 ppm in 3 min, while the Ti content gradually decreased from 0.272 to 0.235 wt% for 20 min. This result indicates that the subsequent addition of Ti reduced the formed alumina inclusions after the Al deoxidation. Therefore, the change of Al and Ti concentration can be described by the forward reaction of the following equation:

$$Al_2O_3(s) + 2\underline{Ti} = Ti_2O_3(s) + 2\underline{Al} \tag{19}$$

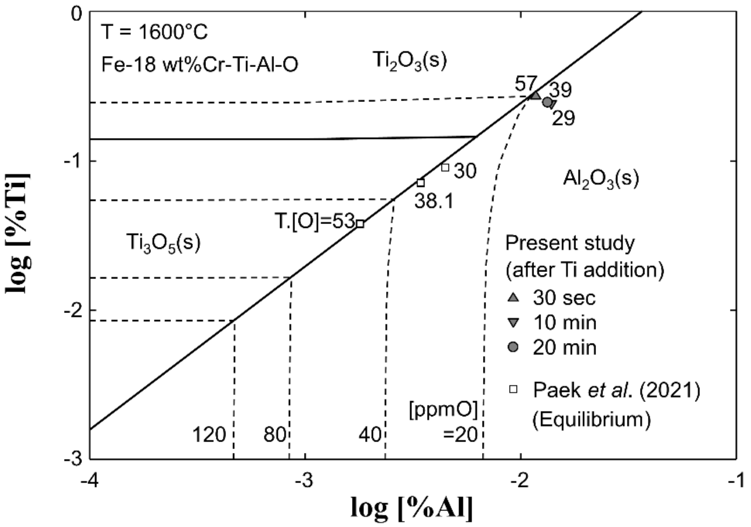

Figure 6. Calculated predominance diagram for oxide inclusions in Fe-18 wt%Cr-Ti-Al-O system at 1600 °C along with the experimental results.[12]

Table 3. The change of melt composition during Al-Ti complex deoxidation in Fe-18 wt%Cr-Ti-Al-O melt at 1600 °C.

Sample number	Time(min)	Addition	[%Al]	[%Ti]	[%O]
Al-0	0	Al	0	0	0.0277
Ti-0	8	Ti	0.007	0	0.0039
Ti-0.5	8.5	-	0.012	0.272	0.0057
Ti-1	9	-	0.013	0.269	-
Ti-3	11	-	0.014	0.251	-
Ti-5	13	-	0.014	0.244	-
Ti-10	18	-	0.014	0.239	0.0029
Ti-20	28	-	0.013	0.235	0.0039

Figure 7 shows the SEM images and EDS analysis results of the oxide inclusion formed during the Al-Ti complex deoxidation process. Based on the thermodynamic stability of Ti oxide inclusions (Figure 6), it was considered as the Ti_2O_3 phase, thus the Al and Ti contents of the inclusions by EDS were converted to the ratio of Al_2O_3 and Ti_2O_3 in wt%. After 8 min of Al addition, only typical Al_2O_3 inclusions were found (Figure 7a). After the Ti addition, the core-shell type of Al_2O_3-TiO_x inclusions was observed along with the polygonal shape of Al_2O_3 inclusions.

The core-shell type of inclusions was composed of the Al_2O_3-rich dark inner part and the grey layer of surrounding TiO_x-rich oxide (Figures 7b). The formation of such a complex dual-phase by the addition of Ti can be attributed to the reduction of alumina at the outer layer of the inclusion which directly contacted liquid steel. Such primary reaction of the outer layer can also be explained by Equation (19). The core-shell structure was completely disappeared in 5 min of Ti addition. After that, only polygonal shapes of Al_2O_3- and TiO_x-rich oxide inclusions were observed as shown in Figures 7c and d. The mutual solubility between these two oxides gradually decreased with time. Finally, the solid Al_2O_3 and TiO_x-rich oxide inclusions coexisted in Fe-18 wt%Cr-Ti-Al-O melt.

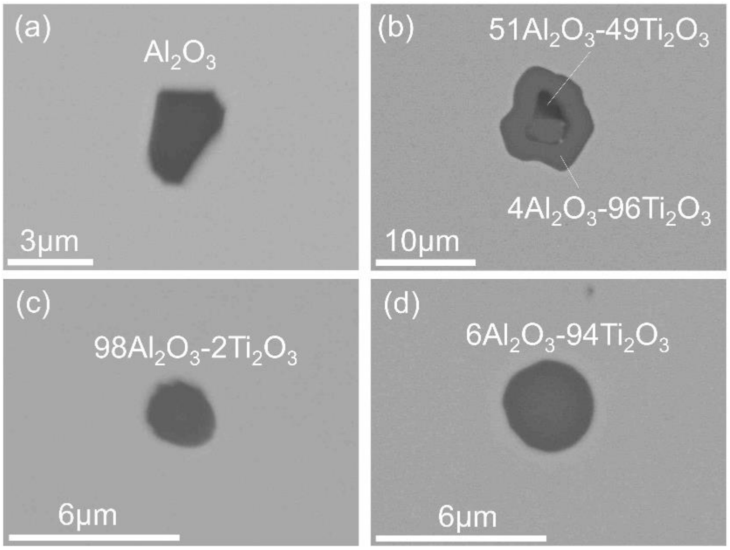

Figure 7. Morphology change of oxide inclusions with time: a) pure Al_2O_3 at 8 min after Al addition, b) core-shall type at 1 min, c) Al_2O_3-rich inclusion at 5 min, and d) Ti_2O_3-rich inclusion at 5 min after Ti addition.

4. Conclusions

The consistent set of interaction parameters were selected for the multicomponent Fe-Cr-Ti-Al-N-O system. The verification experiments checked the compatibility of the parameters in Fe-Cr-Ti-Al-N and Fe-Cr-Ti-Al-O melts, respectively. The N solubility and the solubility product of TiN and AlN were reproduced successfully in the Fe-Cr-Ti-Al-N melts by using the tabulated thermodynamic values. The various types of TiN inclusions, such as Ti oxy-nitride and oxy-carbo-nitride phases, were detected with the Cr and Al solubilities in Fe-Cr-Ti-Al-N melt. The deoxidation equilibria in Fe-Cr-Ti-O and Fe-Cr-Al-O melts were also reproduced well with considering the interaction parameters determined by the nitride equilibration technique. At the initial stage of Al-Ti complex deoxidation in liquid Fe-Cr alloy, the core-shell type of Al_2O_3-Ti_2O_3 inclusion was formed. This dual shape of inclusion was disappeared over time, and then the Al_2O_3- and Ti_2O_3-rich inclusions coexisted in Fe-Cr-Ti-Al-O melt. The change of stable oxide phases and melt composition corresponded well with the equilibrium reaction of Al-Ti complex deoxidation and the constructed predominance diagram in the Fe-Cr-Ti-Al-O system.

Acknowledgements

Open access funding provided by Aalto University. Starting grant from the School of chemical Engineering, Aalto University is greatly appreciated.

Conflict of Interest

The authors declare no conflict of interest.

References

[1] T. Koseki, H. Inoue, Y. Fukuda, A. Nogami, *Sci. Technol. Advanced Materials* **2003**, *4*, 183.
[2] W.Y. Kim, C.O. Lee, C.W. Yun, J.J. Pak, *ISIJ Int*. **2009**, *49*, 1668.
[3] W. Gordon, A. van Bennekom, *Mater. Sci. Technol*. **1996**, *12*, 126.
[4] H. Fujimura, S. Tsuge, Y. Komizo, T. Nishizawa, *Tetsu-to-Hagané* **2001**, *87*, 707.
[5] J.H. Park, *CALPHAD* **2011**, *35*, 455.
[6] E. Shibata, S. Egawa, T. Nakamura, *ISIJ Int*. **2002**, *42*, 609.
[7] M. Matsuo, *Bull. Jpn. Inst. Met*. **1980**, *19*, 192.
[8] C. Wagner, Thermodynamics of Alloys, Addison-Wesley Press, Cambridge, MA **1952**, pp. 47–51.
[9] M.K. Paek, H.S. Son, J.M. Jang, J.J. Pak, *ISIJ Int*. **2020**, *60*, 640.
[10] J.O. Jo, M.S. Jung, J.H. Park, C.O. Lee, J.J. Pak, *ISIJ Int*. **2011**, *51*, 208.
[11] J.O. Jo, W.Y. Kim, C.O. Lee, J.J. Pak, *ISIJ Int*. **2010**, *50*, 1373.
[12] M.K. Paek, J.M. Jang, J.O. Jo, L. Holappa, J.J. Pak, *Metall. Mater. Trans. B* **2021**, DOI: 10.1007/s11663-020-02011-7.
[13] J.M. Jang, S.H. Seo, J.S. Han, D.S. Kim, Y.B. Kang, J.J. Pak, *ISIJ Int*. **2015**, *55*, 2318.

[14] J.J. Pak, J.O. Jo, S.I. Kim, W.Y. Kim, T.I. Chung, S.M. Seo, J.H. Park, D.S. Kim, *ISIJ Int*. **2007**, *47*, 16.
[15] T. Yoshikawa, K. Morita, *Metall. Mater. Trans. B* **2007**, *38B*, 671.
[16] W.Y. Cha, T. Miki, Y. Sasaki, M. Hino, *ISIJ Int*. **2006**, *46*, 987.
[17] D. Janke, W.A. Fischer, *Arch. Eisenhuttenwes*. **1976**, *47*, 195.
[18] A.M. Smellie, H.B. Bell, *Can. Metall. Q*. **1972**, *11*, 351.
[19] R.J. Fruehan, *Metall. Trans*. **1970**, *1*, 3403.
[20] Y. Kojima, M. Inouye, J. Ohi, *Arch. Eisenhuttenwes*. **1969**, *40*, 667.
[21] W.Y. Kim, J.O. Jo, T.I. Chung, D.S. Kim, J.J. Pak, *ISIJ Int*. **2007**, *47*, 1082.
[22] Z. Morita, K. Kunisada, *Tetsu-to-Hagané* **1977**, *63*, 1663.
[23] D.B. Evans, R.D. Pehlke, *Trans. Metall. Soc. AIME* **1965**, *233*, 1620.
[24] M.K. Paek, J.M. Jang, H.J. Kang, J.J. Pak, *ISIJ Int*. **2013**, *53*, 535.
[25] W.Y. Kim, C.O. Lee, C.W. Yun, J.J. Pak, *ISIJ Int*. **2009**, *49*, 1668.
[26] R.D. Pehlke, J.F. Elliott, *Trans. Metall. Soc. AIME* **1960**, *218*, 1088.
[27] L.E. Rohde, A. Choudhury, M. Wahlster, *Arch. Eisenhuttenwes*. **1971**, *42*, 165.
[28] H. Sakao, K. Sano, *J. Japan Inst. Metals* **1959**, *23*, 671.
[29] T. Itoh, T. Nagasaka, M. Hino, *ISIJ Int*. **2000**, *40*, 1051.
[30] A. Sieverts, G. Zapf, H. Moritz, *Z. Phys. Chem. Abt. A* **1939**, *183*, 19.
[31] M.K. Paek D. Lindberg, J.J. Pak, *Vacuum* **2020**, *182*, 109726.
[32] M. Hillert, *J. Alloys Comp.* **2001**, *320*, 161.
[33] S.H. Seok, T. Miki, M. Hino, *ISIJ Int*. **2009**, *49*, 1850.

Table captions:

Table 1. The first- and second-order interaction parameters in Fe-Cr-Ti-Al-N-O system.

Table 2. EDS analysis of extracted nitride inclusions from Fe-18 wt%Cr-Ti-Al-N melt.

Table 3. The change of melt composition during Al-Ti complex deoxidation in Fe-18 wt%Cr-Ti-Al-O melt at 1600 °C.

Figure captions:

Figure 1. Calculated a) Ti-N and b) Ti-O relation at 1600 °C in liquid iron along with the experimental results.[13-23]

Figure 2. Calculated a) TiN and b) AlN solubility product in liquid Fe-Cr alloys along with the present experimental results.

Figure 3. Calculated N solubility and TiN solubility product in Fe-18 wt%Cr-0.28 wt%Al-Ti-N melt at 1550-1700 °C along with the present experimental result at 1700 °C under 0.01 atm.

Figure 4. SEM images of extracted nitride inclusions from Fe-18 wt%Cr-0.28 wt%Al-Ti-N melt a & b) at 1650 and c & d) 1550 °C during cooling.

Figure 5. Calculated a) Ti-O and b) Al-O relation in liquid Fe-Cr alloys at 1600 °C along with the experimental results.[12,15,33]

Figure 6. Calculated predominance diagram for oxide inclusions in Fe-18 wt%Cr-Ti-Al-O system at 1600 °C along with the experimental results.[12]

Figure 7. Morphology change of oxide inclusions with time: a) pure Al_2O_3 at 8 min after Al addition, b) core-shall type at 1 min, c) Al_2O_3-rich inclusion at 5 min, and d) Ti_2O_3-rich inclusion at 5 min after Ti addition.